

NASA TM XE 55451

NEAR INFRARED SOLAR ECLIPSE OBSERVATIONS

GPO PRICE \$ _____

CFSTI PRICE(S) \$ _____

Hard copy (HC) 2.00

Microfiche (MF) .50

653 July 65

BY
**JOHN MANGUS
RALPH STOCKHAUSEN**

FACILITY FORM 808	N66 24643	_____
	(ACCESSION NUMBER)	(THRU)
	<u>34</u>	_____
(PAGES)	(CODE)	
<u>TMX-55451</u>	<u>30</u>	
(NASA CR OR TMX OR AD NUMBER)	(CATEGORY)	

JANUARY 1966



**GODDARD SPACE FLIGHT CENTER
GREENBELT, MARYLAND**

NEAR INFRARED SOLAR ECLIPSE OBSERVATIONS

PURPOSE

This experiment was conceived of as a spectral survey of coronal and chromospheric emission lines in the 1μ to 3.5μ range. The coronal emission lines of Fe XIII have already been observed at 10742\AA and 10798\AA and, on the basis of satellite observations of far UV coronal lines, one would expect similar transitions of other ions to be observed at longer wavelengths.

OBSERVATIONAL CONSTRAINTS

The May 1965 Solar Eclipse Expedition afforded an excellent opportunity for viewing the solar corona and chromosphere (without a coronagraph) from an altitude above 85 percent of the atmospheric water vapor. However, the predicted lines were quite weak (less than 10^{-10} watts/cm²) and expected to appear only as small emission features superimposed on an intense continuum. It was therefore necessary to maximize the spectral irradiance within a resolution element due to an emission line by taking advantage of the circular symmetry of the field with a slitless instrument, selecting a resolving power which would yield an acceptable line to continuum ratio and selecting a detector which would yield an adequate signal to noise ratio. It was also considered desirable to utilize a rapid scanning instrument, one scan per second, in order to detect rapid events

during the eclipse. Finally, a total field angle of 72 arc minutes was selected in order to compensate for the predicted aircraft roll of ± 15 arc minutes with a manual pointing control and at the same time not vignetting the 6 arc minute annular field of interest adjacent to the solar disc.

INSTRUMENTATION

A Michelson type scanning interferometer was selected as the best type of instrumentation to fulfill the slitless, spectral, spatial and scanning requirements. Figure 1 illustrates the optical layout of the infrared Michelson type scanning interferometer which was used on the eclipse¹. The instrument consists essentially of two interferometers with compensating plates. One receives the coronal flux and is called the "scanning interferometer", the other is called the "monitoring interferometer". As shown, two mirrors, one in each arm of the two interferometers, are rigidly connected together on a transducer. The transducer moves the mirrors at a constant velocity through a total displacement of one millimeter in one second. Stationary phase is located centrally in the mirror displacement thereby yielding a total retardation of 1000 microns or a resolution of 20 kaysers at 10000 kaysers.

¹Manufactured by Block Engineering, Inc., under NASA

Contract NASA 5-9127

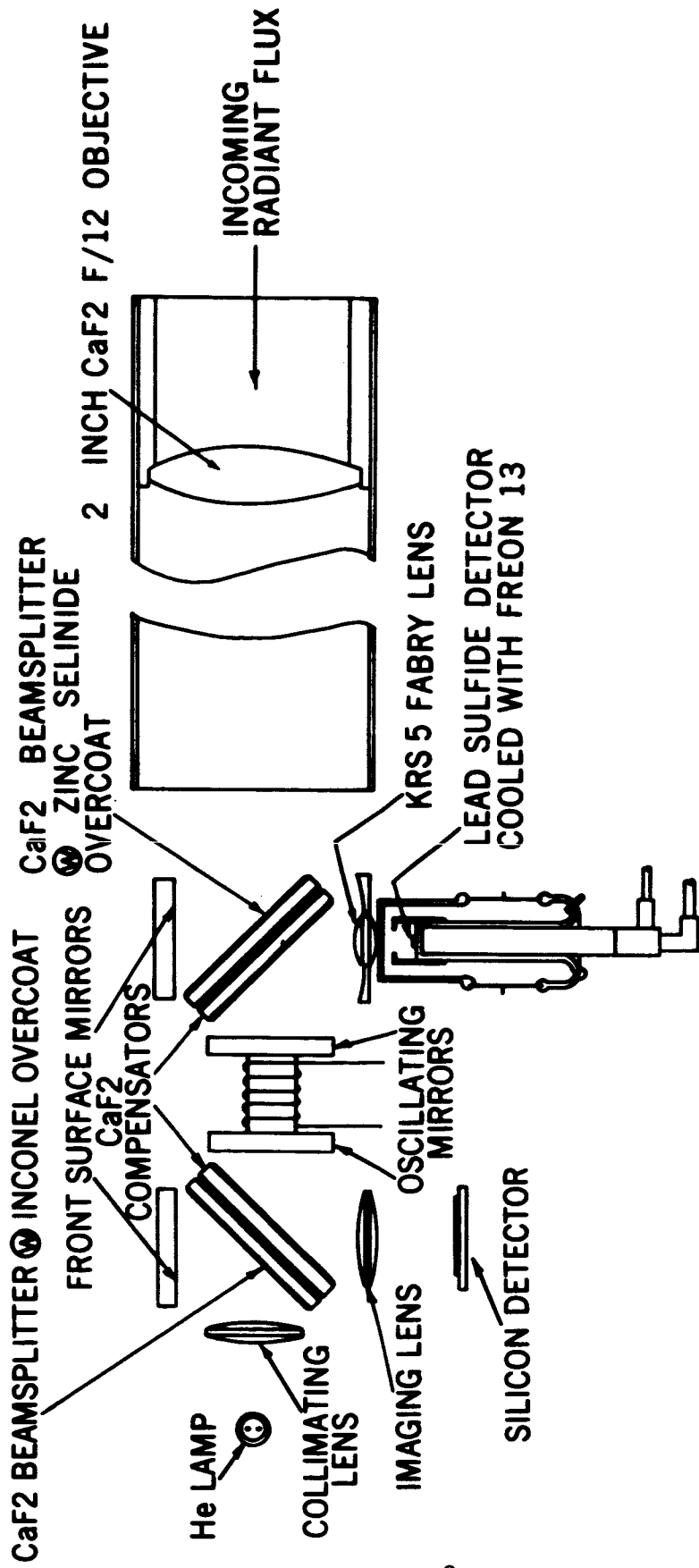


Figure 1 - Infrared Michelson - Type Scanning Interferometer

The two inch diameter calcium flouride lens, which is the entrance aperture of the scanning interferometer, is imaged on a freon 13 cooled (193 °K) lead sulfide detector by a KRS5 Fabry lens. This optical technique of imaging the entrance aperture on to the detector nullifies the effect of variation in response across the face of lead sulfide crystal and at the same time allows variation in the centering of the field about the pointing vector. A spherical mirror, concentric with the Fabry lens, minimizes the effects of scattered light by permitting the detector to see only itself (i.e. - the detector is located at the radius of curvature of the mirror).

Oscillation of the mirror in the scanning interferometer at the one cycle per second rate causes the incident flux to be interferometrically modulated and thereby detected as a point to point summation in time of the amplitudes of the discrete audio frequencies associated with each optical wavelength transmitted by the instrument. This resultant amplitude or voltage versus time output signal of the interferometer is known as the interferogram.

The monitoring interferometer incorporates its own source, the 10830Å line from a helium lamp. Because only one wavelength is modulated in this case, the output of the interferometer, the interferogram, has the form of a sine wave with a frequency of about 917.2 cps. The output from this interferometer, as shown in Figure 2, is phase compared with a matched oscillator

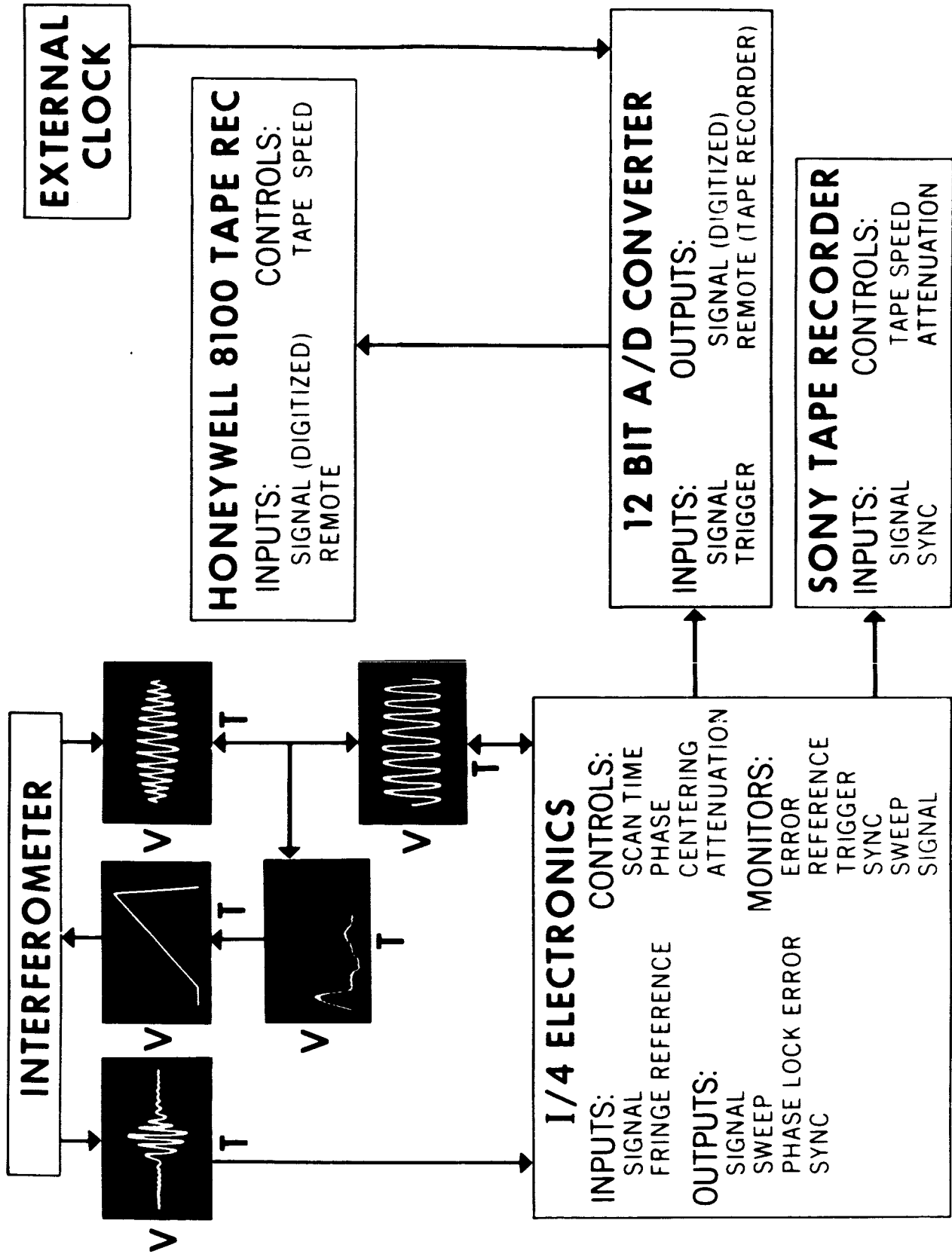


Figure 2 - Interferometer Phase Lock and Data Flow Collection Scheme

in the I/4 electronics. The resultant error voltage is applied as a correction to the transducer ramp or sweep voltage. This technique was used to preserve the average linearity in the mirror displacement when the instrument was mounted on board the NASA-AMES Convair 990 aircraft².

The interferogram from the scanning interferometer was recorded in two ways. First the signal and a sync pulse were recorded in analog form on a two track Sony Model 250A tape recorder. Secondly, the signal was fed into a 12 bit analog to digital converter and digitized to an accuracy of one part in 4096 for a peak to peak voltage of 0 to - 10 volts. The output of the 12 bit analog to digital converter is generated in a standard IBM format and recorded on a modified Honeywell 8100 tape recorder at 556 bits per inch. The first data word in each record is a time code, generated by the on-board Chrono-Log Model 20,000 Time Code Generator. The output of this clock was also used to trigger a Nikon F 250 frame 35 millimeter camera. The above camera was mounted on the back of a Questar telescope which was boresighted with the interferometer. It was planned to correlate these exposures of the eclipse with coincident interferograms.

²For a more detailed account of the instrumental design, theory and projected improvements see, Near IR Eclipse Instrumentation by A.L. Lavery, Block Engineering, Inc., also published in these Proceedings.

However, 60 seconds before second contact a power failure occurred in the camera circuitry. Some exposures were obtained as shown in Figures 3A and 3B by using a manual exposure mode but these photographs could not be correlated with particular spectral scans. The film used in the camera was Extended Range Film manufactured by Edgerton, Germeshausen and Grier, Inc., Figure 3A and 3B are prints of a 1/60 second exposure. Figure 3A was printed using the XR negative with a Kodak wratten filter #48A. Figure 3B was printed using the same negative, with a Kodak wratten filter #85.

AIRCRAFT MOUNTING

The interferometer and Questar were mounted in the aircraft as shown in Figure 4. The interferometer was shock mounted to an azimuth - elevation manual pointing control. This control proved satisfactory for maintaining the required pointing accuracy of ± 15 arc minutes.

The interferometer viewed the eclipse through a six inch diameter, one inch thick calcium flouride window which had a transmission of 93 percent from one to four microns. This window was quite easy to keep clean and did not evidence any severe fogging or hydroscopic activity.

Shock mounts to the electronics cabinet had to be by-passed to meet the 9g loading requirements, however, there was no noticable increase in the instruments' susceptibility to aircraft vibration.

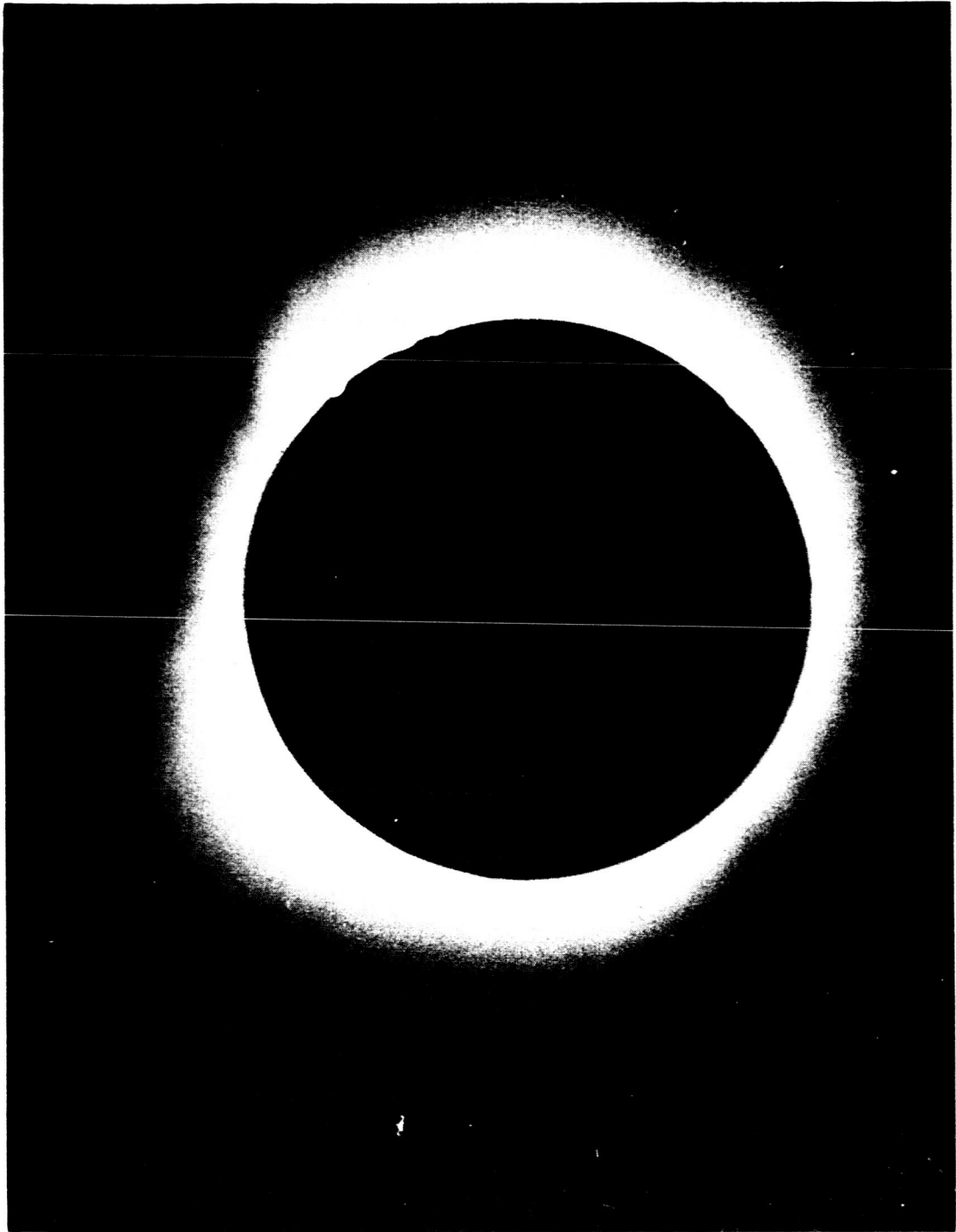


Figure 3a

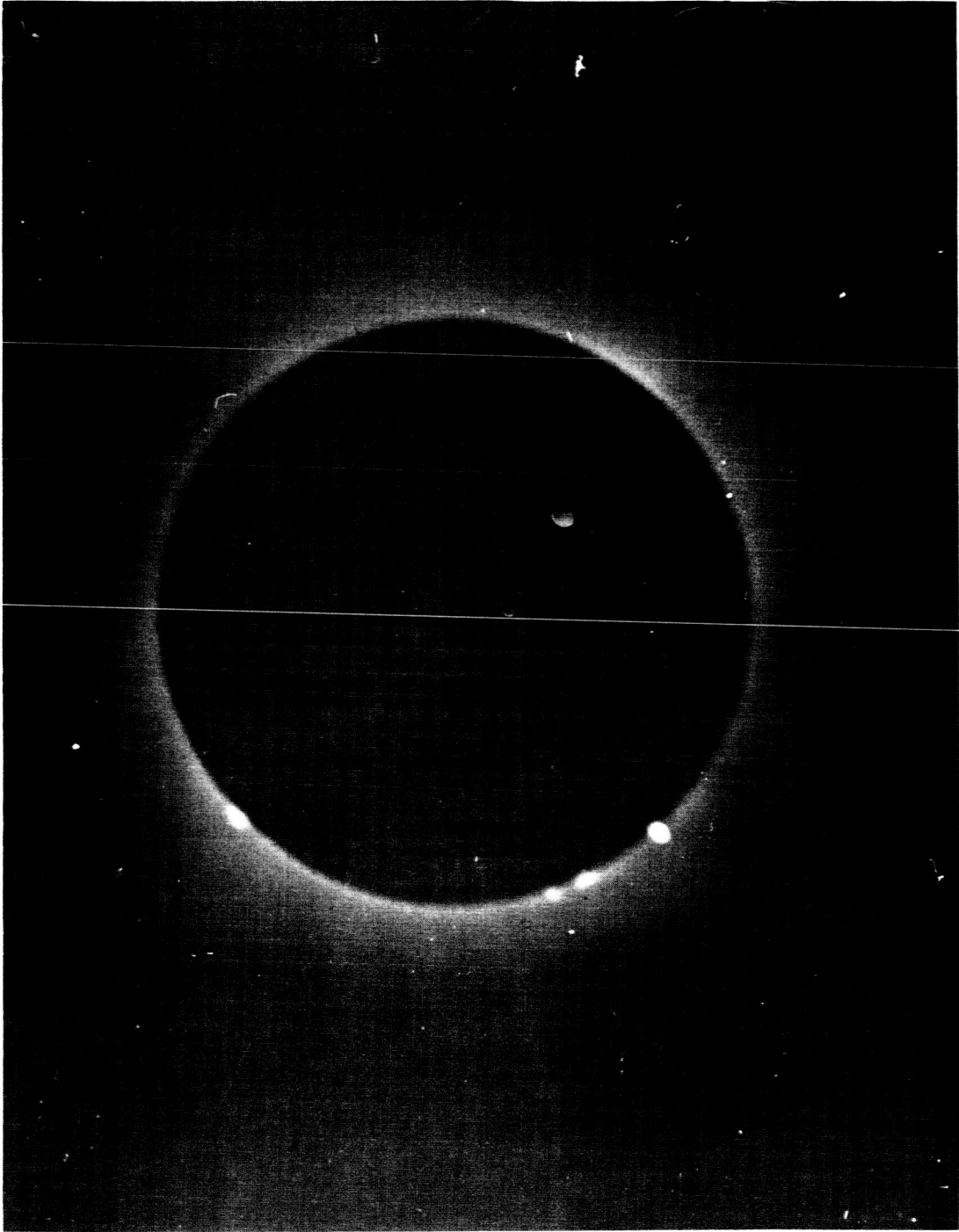


Figure 3b

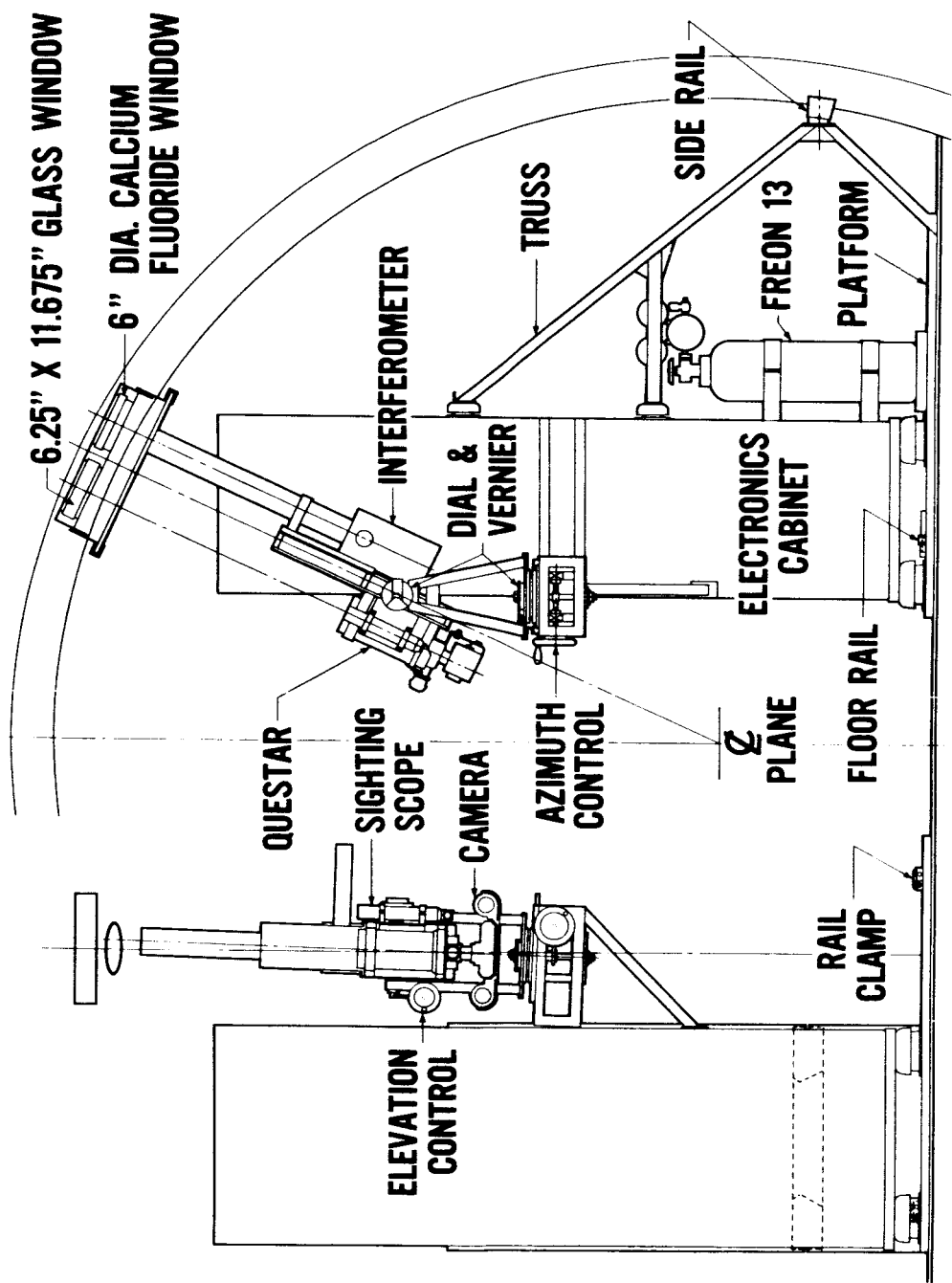


Figure 4 - Mount for Airborne Eclipse Interferometer

DATA REDUCTION

The interferogram can be represented by the following relation:

$$I(t) \propto \int_{\omega_{\min}}^{\omega_{\max}} B(\omega) \cos \omega t \, d\omega.$$

$B(\omega)$ represents spectral irradiance of the light source, t is the time and ω is the angular frequency. This angular frequency is proportional, with different proportionality factors, to both the electrical frequency of the detector output and the wavenumber of the light.

The spectrum can be obtained by performing a cosine Fourier transform on the interferogram. This operation can be expressed

$$B_C(\omega) \propto \int_{-T/2}^{T/2} I(t) \cos \omega t \, dt$$

where T is the time interval of one mirror scan. For the case where the interferogram has been sampled at discrete time intervals and digitized, the spectrum can be represented

$$B_C(\omega) \propto \sum_{n=-N/2}^{+N/2} I(n\Delta t) \cos (\omega n\Delta t)$$

where Δt is the sampling interval, n is the time parameter and $N + 1$ is the total number of samples in the time of one mirror scan.

For two reasons, the cosine transform alone is not adequate. Since the mirror motion is not coupled with the sampling circuits and because the mirror motion is not always symmetrical about

the "zero" position of the mirror, the interferogram sample at $n = 0$ does not always correspond to the mirror position for zero phase difference. Performing only a cosine transform under these conditions will result in a distortion of the spectrum. Connes (1961) has shown that this problem is eliminated by performing the complete (sine and cosine) Fourier transform.

The computer program used in the data reduction was supplied by Block Engineering, Inc. but was extensively modified by Goddard. The computational scheme used can be expressed,

$$B_C(m) \propto \sum_n I(n) \cos(mn\theta) \equiv \sum_n P(m,n)$$

where m is the wavenumber parameter and θ depends on various system parameters. In the actual computation, n varies from about -1000 to +1000 while the range of m is about 1 to 3000. The following recursion formula is used to generate the cosines:

$$\cos(m+1)\varphi = 2 \cos\varphi \cos m\varphi - \cos(m-1)\varphi$$

The following matrix shows schematically the computational procedure

$m \backslash n$	-1000	-999	...	+1000	\sum_n
1	P(1,-1000)	P(1,-999)	...		B(1)
2	P(2,-1000)	P(2,-999)	...		B(2)
⋮	⋮	⋮			
3000				P(3000,1000)	B(3000)

The procedure is to generate each column by the recursion formula and then sum each row to obtain $B_C(m)$. A similar procedure

is used for the sine transform. One can see that for high n and m values there are well in excess of 10^6 mathematical operations (additions, multiplications, etc) performed in generating each $B(m)$. It is, therefore, necessary to be concerned with truncation errors. The final form of the program was compared with a double precision run. The maximum error in the total transform, $(B_c^2 + B_s^2)^{1/2}$, was about 3 or 4%.

SPECTRAL CONTAMINATION

A common problem in spectroscopy, but especially in Fourier transform spectroscopy, is spectral contamination by spurious features. Figure 5 shows an average of twenty-three spectra obtained by covering the fore optics. (The spectral plots appear to be analog, but this is a result of plotting machine. There are actually 200 real data points between vertical grid lines. The abscissa is the parameter m mentioned above. Multiplication by 3.418 gives the approximate wavenumber in kaysers. Each plot was normalized so as to make use of the full dynamic range of the plotting device.) With the fore optics covered, the spectrum should be composed of an r.m.s. noise level, the self-emission of the instrument and any spurious instrumental effects. The continuum in the range $m = 600$ to $m = 1200$ is thought to contain a contribution from the instrumental self-emission, but it is probably mostly due to the thermal emission of the object used to cover the fore optics, since a continuum of this magnitude is not observed when the fore optics are uncovered. The general continuum over the entire spectrum

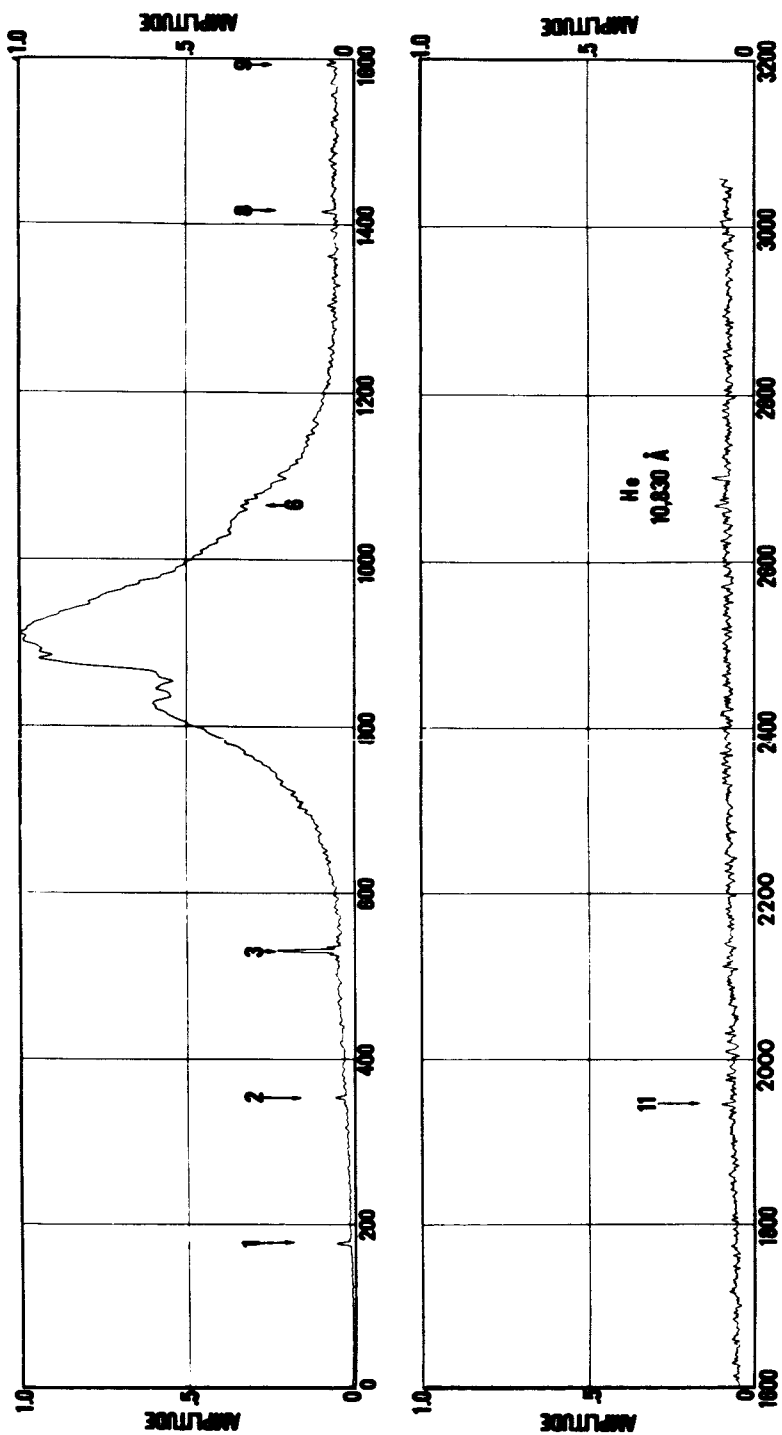


Figure 5 - Noise and Instrumental Spectrum Average of Twenty-three Scans. Normalization Factor = 1.122.

is the r.m.s. noise level. It should be pointed out that the spectra displayed in this paper have not been corrected for the effects of wavenumber (or frequency) response. In addition to the continuum, several "emission" features can be seen. The numbered arrows indicate the positions of the harmonics of 60 cps. None of the emissions which have been identified as solar lines correspond to the positions of these harmonics. The "emission" labeled Hel10830Å is probably an effect due to the control interferometer. The monochromatic light source used in the control interferometer was the helium 10830Å line and it is possible that a small signal of the corresponding electrical frequency has been added to the interferometer output through the electronic circuitry. However, this spurious emission seems to be always small compared to the solar emission line.

In addition to the "emission" features discussed above, a number of large amplitude features occasionally occur at positions corresponding to frequencies of 1 cps to 20 cps. These have been interpreted as being due to the mechanical vibrations of the airplane plus interferometer mount. However, it has never been observed that these "emissions" have extended into the spectral region of interest.

Probably the most serious spurious effects are due to side lobes and side bands of the true emission lines. Because of the finite (instead of infinite) displacement of the movable mirror, the Fourier transform is performed over a finite interval. As

a result, true emission lines will be accompanied by a series of side lobes. These are obvious in the case of a bright emission line such as the one at $m = 2700$ in Figure 6. For the case of weak lines, the side lobes are probably below the noise level. Side bands seem to be an even more serious problem because they can occur at fairly large distances from the true emission line. The emission features located at about $m=2600$ and $m=2800$ could possibly be side bands, however, more work needs to be done in order to definitely eliminate these features as true emission lines. Side bands could be formed by some amplitude or frequency modulation of the signal.

A theoretical study has been made of the effects of an amplitude modulation on the signal. The actual interferogram $I(n)$ was read into the computer and modified as follows:

$$I'(n) = M(n) \cdot I(n)$$

where $M(n)$ is a modulating function generated in the computer. Two functions have been considered:

parabolic:	$M(n) = p(n-q)^2 + h$
exponential:	$M(n) = a \text{ EXP}(bn)$

Physically, the parabolic modulation might be produced by a loss of guiding, where the sun drifted across the field of view during one spectral scan. The exponential modulation might represent the actual time decay of the coronal brightness as the corona becomes occulted by the moon. In all the cases studied the maximum value of $M(n)$ was taken to be 1.01 times

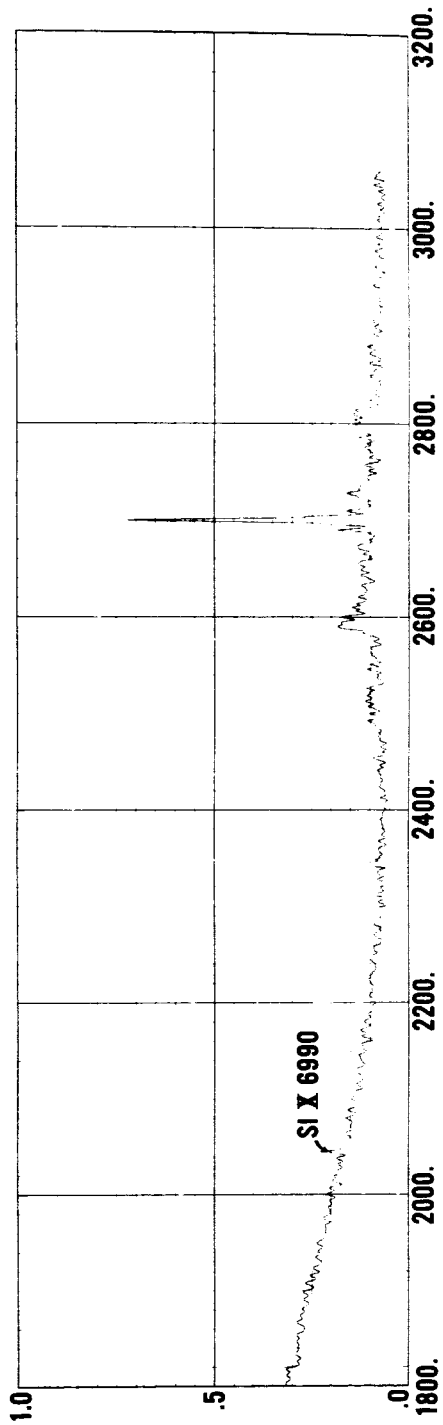
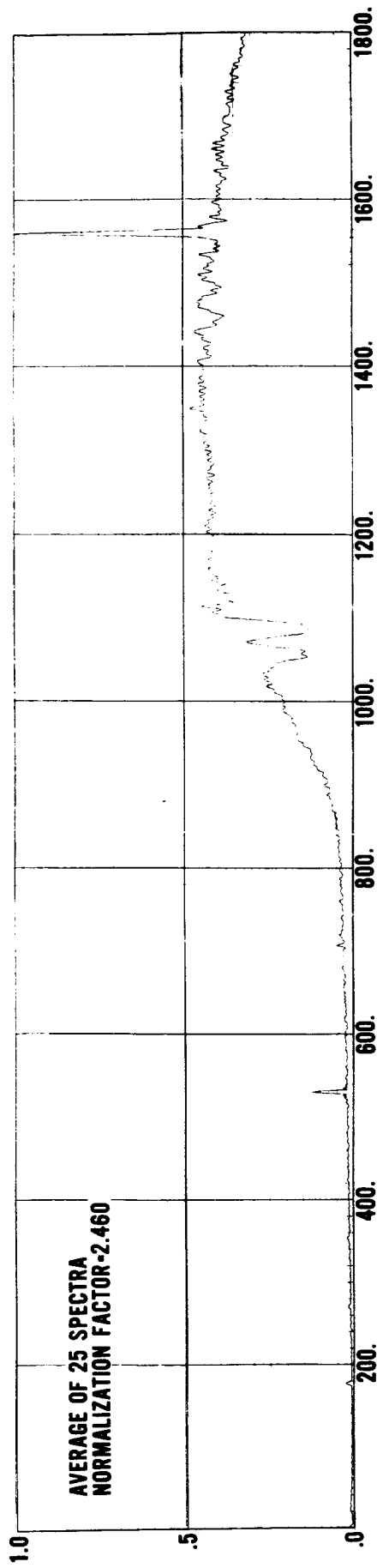


Figure 6 - Average of Twenty-five Spectral Scans.

the average value of $I(n)$, i.e. a rather small amplitude modulation. The Fourier analysis of the modified interferogram yields an unmodified spectrum, except for a large "emission line" at approximately zero frequency. No such feature has been observed in any of the eclipse spectra, so we would like to conclude that time variations of the observed radiation had no effect on the spectra. However, it must be remembered that this theoretical investigation is only an approximation. It does not take into account the fact that the low frequency gain of the amplifiers is very low and also that it is possible that some mixing of signals in the amplifiers might produce side bands. We are planning laboratory studies to settle these questions.

WAVENUMBER CALIBRATION

A number of independent schemes were used to determine the wavenumber scale. Laboratory and in-flight spectra of the emission lines of neon were obtained. The structure of the CO₂ atmospheric absorption bands observed in the eclipse spectra were compared with observations by Houghten et. al. (1961). Houghten's spectra were obtained by observing the uneclipsed sun from an altitude of 40000 ft. with a resolution of about 1 cm^{-1} . Finally, the hydrogen emission lines observed in the eclipse spectra were used to obtain a wavenumber scale factor. These three methods indicate that the wavenumbers are accurate to a couple of percent, quite adequate for this low resolution work.

ECLIPSE SPECTRA

Since the solar emission was considerably less than anticipated, most of the single scans, except near second and third contact are too noisy for reliable interpretation. However, after adding a number of spectra, the noise goes down considerably and the emission lines show up nicely. Figure 7 is an average of seventy spectra taken near third contact. Error bars at two locations show the calculated standard deviation of the mean for those regions. Members of the Paschen and Brackett series of neutral hydrogen and the 9231 kayser (10,830Å) line of neutral helium are readily identified. Figure 6, which is an average of 25 spectra taken near second contact, shows a weak emission line that might possibly be identified as the 6990 kayser line of SiX. This line is a very weak but persistent feature of the spectra. However, at the present state of data reduction its reality is more a matter of faith. There are quite a number of other apparent emission features whose reality will require considerable investigation. Table 1 lists the line identifications made to date. Wavenumbers are given in kaysers.

TABLE I
WAVENUMBER DETERMINATIONS

<u>OBSERVED</u>	<u>POSSIBLE IDENTIFICATIONS</u>
3809	3808.3 Brackett (6-4)
4617	4616.6 Brackett (7-4)
5143	5141.2 Brackett (8-4)

TABLE I (Continued)

<u>OBSERVED</u>	<u>POSSIBLE IDENTIFICATIONS</u>
5329	5331.6 Paschen (4-3)
	5350.7 He ($4^3F - 3^3D$)
	5348.0 He ($4^1F - 3^1D$)
6987	6990 Si X ($2^3P_{3/2} - 2^3P_{1/2}$) ?
9133	9139.9 Paschen (6-3) ?
9230	9230.8 He ($2^3P - 2^3S$)

TIME VARIATIONS

The intensities of the three brightest lines (Paschen (4-3), Brackett (6-4) and He 9231k) were estimated by replacing the area under each line by the area of a roughly fitted triangle. Figure 8 shows the time variation of these lines. The time scale is not accurate to more than a few seconds at present. We were not observing during the first flash, but obtained spectra at the beginning of the second flash, which began at about 555 seconds. Each point represents an average intensity, the numbers of scans averaged is shown in the figure. The points are plotted at the middle of the time interval covered.

Since the lines whose intensities are plotted here probably originate in low temperature regions, they must be from the chromosphere or from prominences. Since they have such a considerable duration they cannot be of chromospheric origin, except during the second flash. Another apparent feature is the strong asymmetry of the time variation, being much brighter

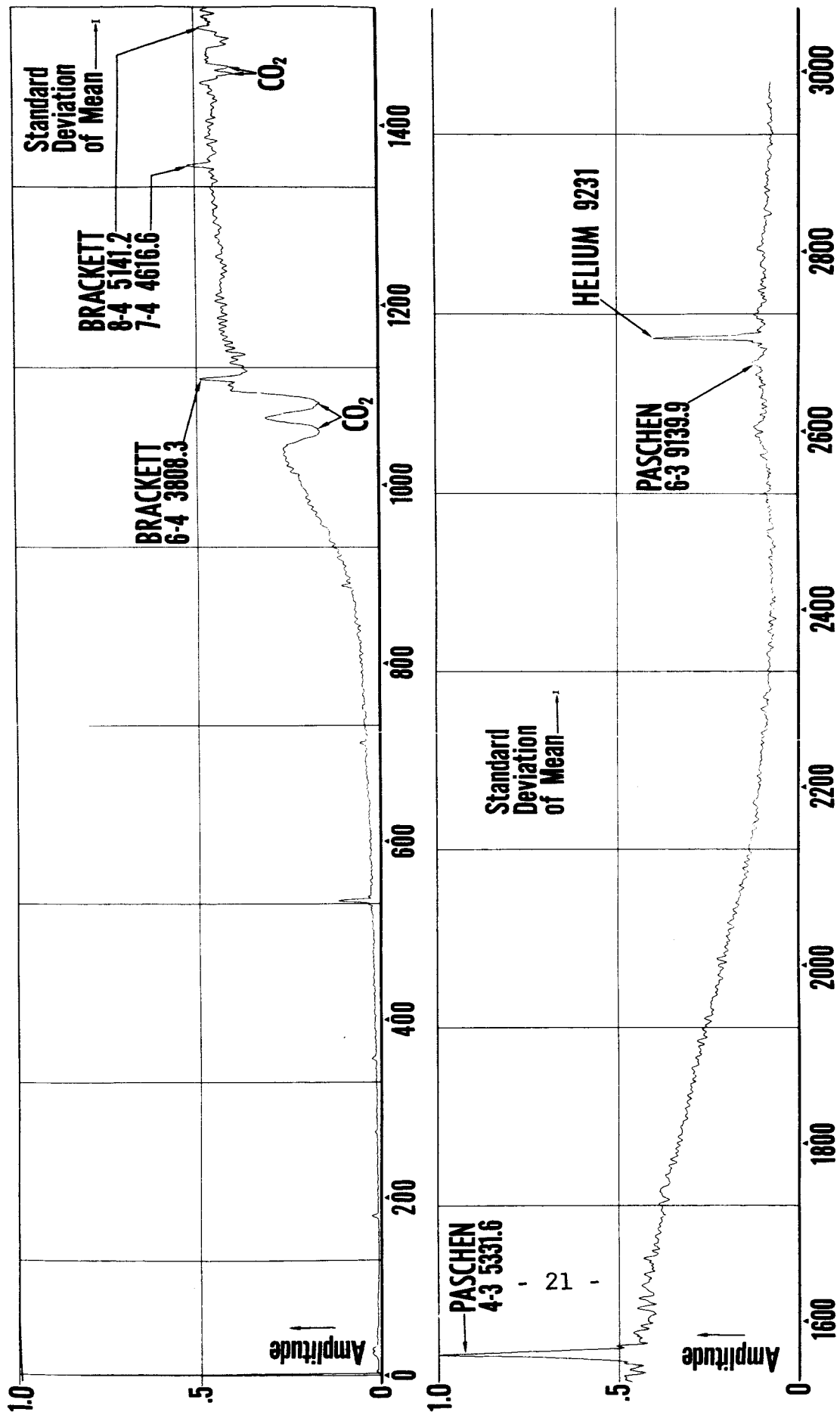
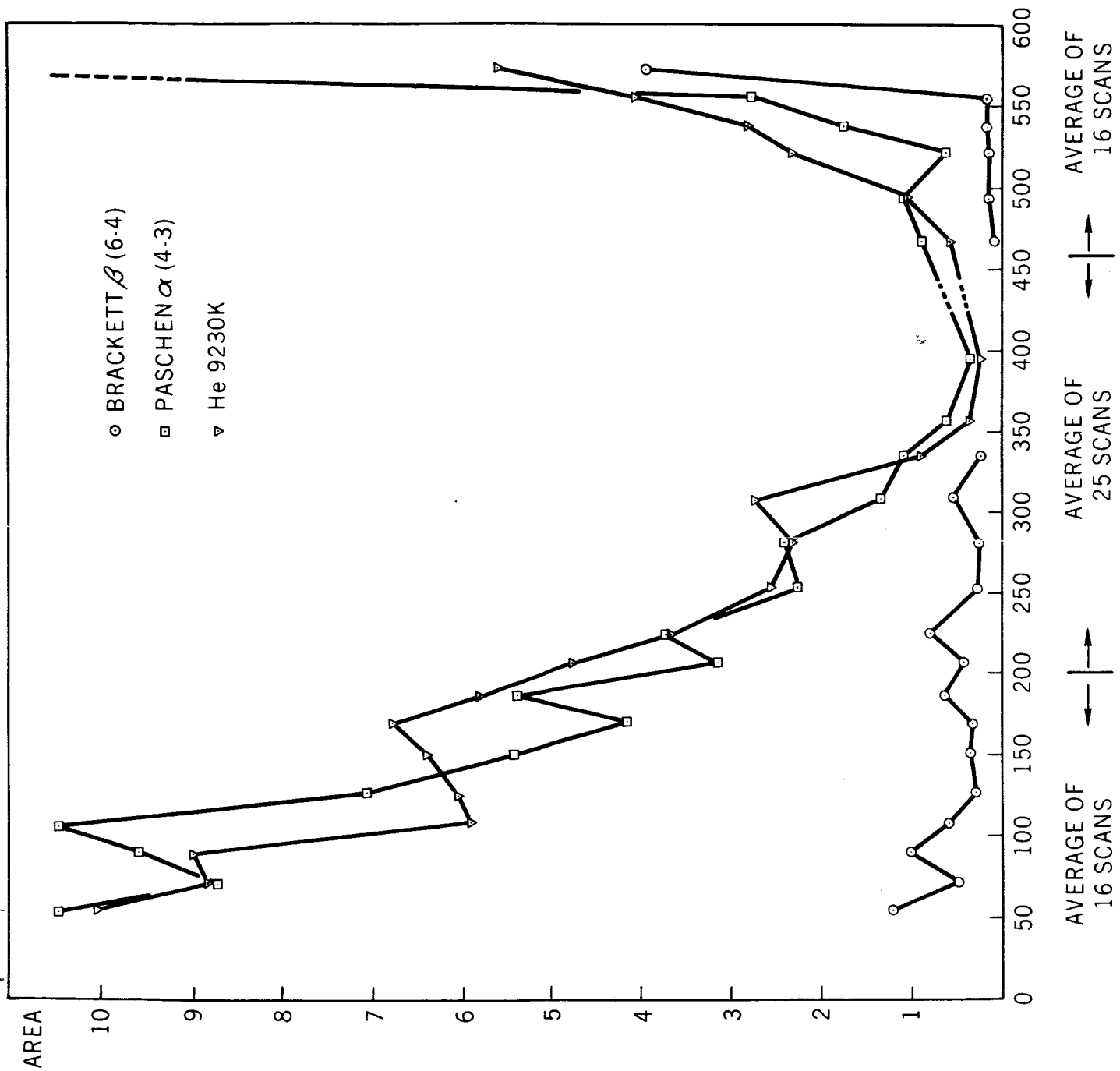


Figure 7 - Average of Seventy Spectral Scans.
 Normalization Factor = 2.477.



after second contact than before third contact. Figure 9, taken from that of W. P. Boquist (whose observations on the AFCRL plane were taken several minutes before ours), shows a similar qualitative behavior in the number and duration of visibility of prominences. We would like to conclude, then, that the lines of neutral hydrogen and helium originated in the prominences except for the flash duration.

The time variation of the total emission received has also been investigated. The ordinate shown in Figure 10 represents the average total area under the curve of each average spectra. This area includes emission lines, instrumental self-emission, and the r.m.s. noise level. These have a negligible contribution (the lines near second and third contact contribute only a few percent). Most of the total emission is a solar (or other) continuum. It is seen that there is little asymmetry in this variation. Also the amplitude of the total emission varies by only about 10% while that of the lines varied by a factor of 10. It seems likely then that most of the continuum does not come from the prominences. Possibly most of it comes from the corona, but a contribution from the atmosphere has not been eliminated.

RELATIVE INTENSITIES

For the purpose of obtaining absolute intensities, the unclipped sun was observed on practice flights several days before and after the eclipse. An aluminum coated, quartz flat

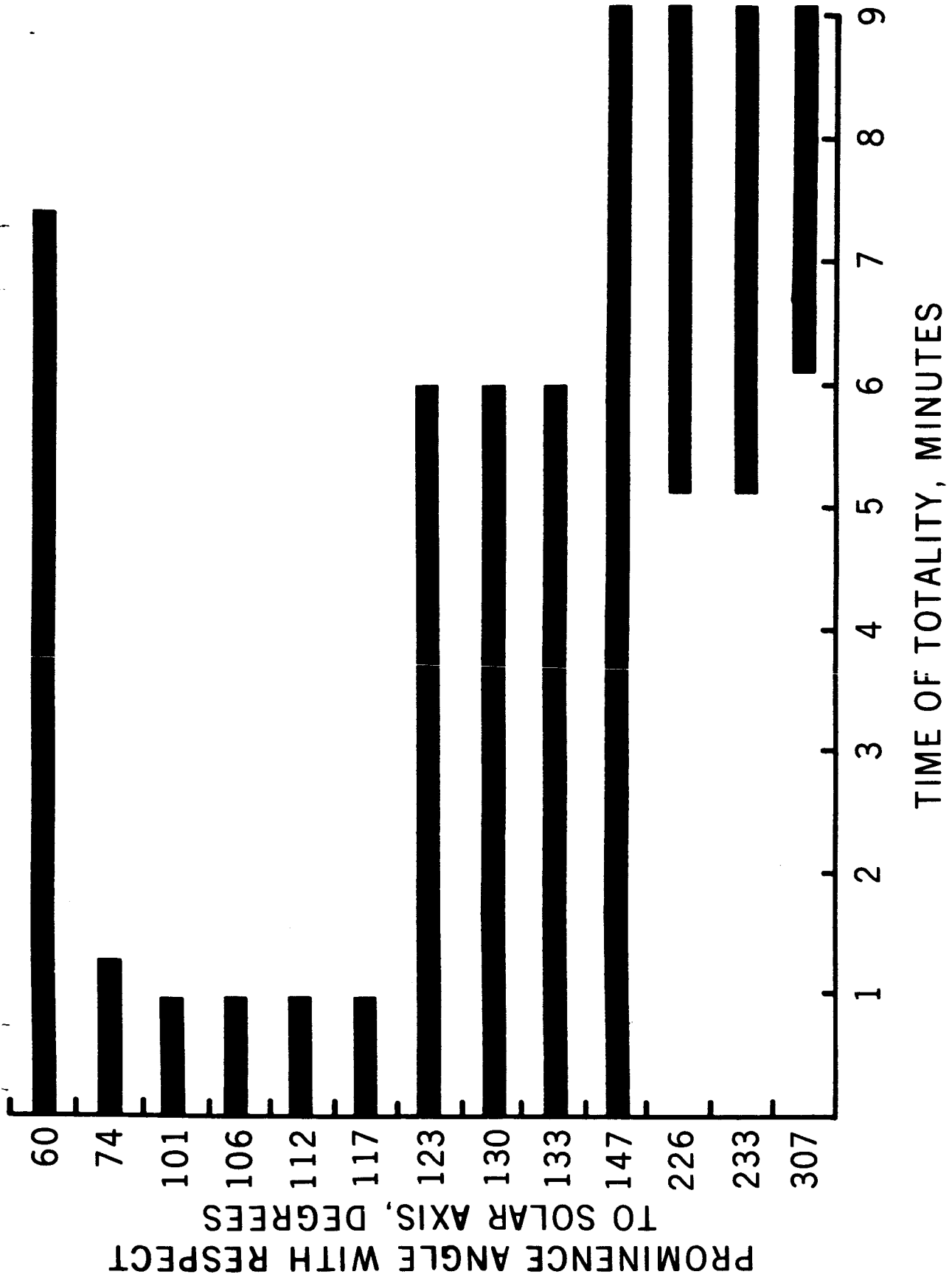


Figure 9 - Duration of Visibility of Solar Prominences. Taken from W.P. Boquist, Sky and Telescope, January, 1966

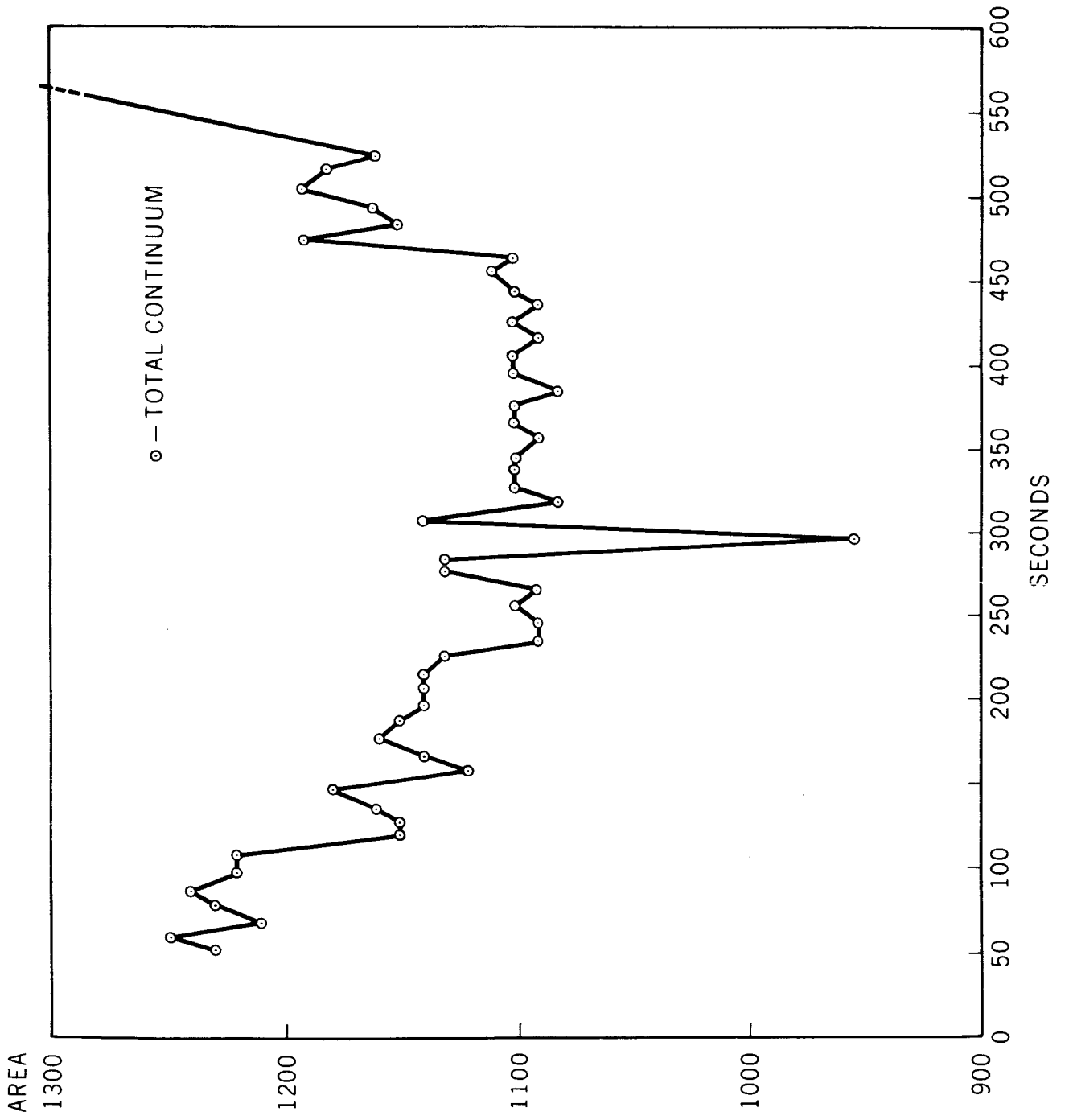


Figure 10 - Time Variation of Total Continuum.

was used as a neutral density filter. Observations of the partially eclipsed sun were also made through this filter. It is hoped that eventually we will be able to obtain the intensities of the lines in terms of the continuum at the center of the solar disc.

At this stage of the reductions we only have available estimates of the relative intensities of the lines. These were obtained by correcting the uneclipsed disc observations for the measured transmission of the neutral density filter. The remainder of the instrumental effects were corrected by comparing our disc observations with those listed by Allen (1963). The relative intensities obtained were:

He 9230	1.0
Paschen (4-3)	.2
Brackett (6-4)	.002

At this stage of the reductions it is difficult to estimate the error of these values, so these intensities should be considered only order of magnitude at present.

FUTURE EXPERIMENTS

We believe that this first attempt at near-infrared eclipse observations using a Michelson interferometer spectrometer has shown the usefulness of airborne astronomical observations with this type of instrumentation. However, a number of modifications are required and we hope to perform this experiment again with larger fore optics, a higher spectral and spatial resolution and faster spectral scans.

We also believe that a continued search for infrared coronal emission lines is desirable. A preliminary search has turned up a moderate number of possible lines in the 1μ to 10μ range. These are listed in Table 2. The first two columns contain the wavenumber and ion, respectively. The third column shows the ionization potential while the fourth shows the product of transition probability with wavenumber of the transition (this gives a rough measure of intensity, but abundance and degree of ionization have to be considered as well). This table was made up by simply searching through Atomic Energy Levels for any ground term magnetic dipole transition which occurred in the 1μ to 10μ range. The transition probabilities were taken from Pasternack (1940). All elements of reasonable solar abundance were included and all stages of ionization. A number of the transitions are very unlikely since they will occur in high density regions where the upper level will be collisionally de-excited. However, even the non-appearance of a line can be useful in setting limits to the chromospheric and coronal structure.

ACKNOWLEDGEMENTS

We would like to thank the following people who made this experiment possible. D. Lavery and G. Wyntjes of Block Engineering, Inc. and W. Poland, K. Saffer and G. Dietz of Goddard for their work on the instrumentation; and N. Paris for his work on the computer programming. We would also like to thank Ames Research Center for their assistance and for the opportunity to participate in the eclipse expedition.

$(\frac{1}{\lambda})$ cm ⁻¹	element	I.P. e.v.	$A \cdot (\frac{1}{\lambda})$ Sec ⁻¹ cm ⁻¹	$(\frac{1}{\lambda})$ cm ⁻¹	element	I.P. e.v.	$A \cdot (\frac{1}{\lambda})$ sec ⁻¹ cm ⁻¹
10000	Mn X	248	2.2 10 ⁵	1780	Mg V	141.2	2.31 10 ²
9900	Cr VIII	185	1.72 10 ⁵	1740	Cr IX	209.6	4.87 10 ²
9302	Fe XIII	355	1.35 10 ⁵	1700	Mn X	248	4.25 10 ²
9258	Fe XIII	355	9.91 10 ⁵	1673	K IV	60.9	1.67 10 ²
7970	S IX	378.95	9.06 10 ⁴	1627	Ca VII	128	1.25 10 ²
7860	Cr IX	209.6	8.65 10 ⁴	1540	Si VII	246.4	2.93 10 ²
6990	Si X	401.3	2.14 10 ⁴	1537	Ni VIII		1.51 10 ²
5100	Si VI	205.1	1.21 10 ⁴	1506	Ni II	18.1	8.33 10 ¹
4305	Ca VIII	147	3.08 10 ³	1432	A II	27.6	7.55 10 ¹
4030	Si VII	246.4	6.05 10 ³	1364	Na III	71.7	6.21 10 ¹
3870	Si IX	351.8	3.03 10 ³	1361	Ni III	36.2	8.93 10 ¹
3304	Mg VIII	266	1.07 10 ³	1355	Mn VII	119	3.64 10 ¹
3129	K VII	118	8.60 10 ²	1332	Ni I	7.6	8.19 10 ¹
3115	Ca IV	67	1.69 10 ³	1316	Ne VI	157.9	2.68 10 ¹
2660	S IX	378.95	2.71 10 ³	1280	Fe VII		5.38 10 ¹
2590	Si IX	351.8	8.08 10 ²	1267	A V	75	3.42 10 ¹
2443	Ca VII	128	4.64 10 ²	1172	Ni VIII		8.18 10 ¹
2404	Ca V	84.4	7.45 10 ²	1160	Na VI	172.4	2.44 10 ¹
2226	Mg IV	109.3	4.41 10 ²	1131	K VI	99.7	2.94 10 ¹
2210	A VI	91	2.14 10 ²	1127	Mg VII	225.3	2.93 10 ¹
2162	K III	46	3.91 10 ²	1113	Co VII		4.14 10 ¹
2139	Na VII	208.4	1.88 10 ²	1112	A III	40.9	3.45 10 ¹
1875	Fe VIII	151	1.34 10 ²	1106	Na IV	98.9	3.32 10 ¹
1812	Mg VII	225.3	1.45 10 ²	1047	Fe VII		3.04 10 ¹
1793	K VI	99.7	1.38 10 ²	1012	Ni VIII		4.52 10 ¹

Table 2 - Line Predictions

BIBLIOGRAPHY

CONNES, J. 1961, Revue d' Optique, 40, 45.

HOUGHTEN, J. T., et. al. 1961 Philosophical Transactions
of the Royal Society of London, 254, 47.

ALLEN, C. W. 1963, Astrophysical Quantities, 2nd ed.
(London: The Athlone Press).

PASTERNAK, S. 1940, Ap. J., 92, 129.